Ultrafast surface strain dynamics in MnAs thin films observed with second harmonic generation

Jesse J. Dean, Christoph Lange, and Henry M. van Driel*
Department of Physics and Institute for Optical Sciences, University of Toronto, Toronto, Ontario M5S 1A7, Canada
(Received 21 October 2013; published 9 January 2014)

Optical second harmonic generation (SHG) is used to probe surface strain in 150 and 190-nm thin films of MnAs grown epitaxially on GaAs(001). The *p*-polarized SHG signal produced by *p*-polarized 775-nm, 200-fs pulses is theoretically and experimentally shown to be sensitive to the normal component of surface strain from −20 to 70 °C, which includes the ferromagnetic/paramagnetic striped coexistence phase region that exists from ∼10 to 40 °C. We use this dependence to time-resolve the surface strain dynamics in MnAs following pumping with 200-fs pulses of 1.0 or 2.0 mJ cm^{-2} that raise the surface temperature by tens of degrees. For a film at −20 °C the strain reaches a minimum value in ∼10 ps, indicative of electron-lattice thermalization, before recovering on a 500-ps time scale consistent with a one-dimensional heat diffusion model. For a film at 20 °C the minimum strain is reached only after ∼200 ps and attains a value higher than predicted by the heat diffusion model; recovery, however, still occurs in ∼500 ps. The long strain fall time possibly reflects the influence of latent heat and stripe dynamics in the coexistence phase. The larger calculated drop in surface strain may be due to deficiencies in the one-dimensional heat diffusion model. The nonequilibrium surface strain also may not be determined by the local temperature alone but by the constraints throughout the film/substrate system, which are certainly known to govern the strain and stripe characteristics under equilibrium conditions.

DOI: 10.1103/PhysRevB.89.024102 PACS number(s): 68.55.−a, 78.47.J−, 42.65.−k, 78.66.−w

I. INTRODUCTION

Thin films with ferromagnetic, ferroelectric, or superconducting properties are at the heart of much of modern technology.[1–4] When there is a difference in the lattice constants of the film versus the substrate bulk materials, i.e., a misfit strain, an elastic strain can occur to retain lattice matching with the substrate over a substantial temperature range and the properties of the heteroepitaxially grown films can differ significantly from those of the bulk material, with, e.g., a very different phase diagram. Although some phases are homogeneous, in some cases domain formation, often spatially periodic, can occur as nonuniform elastic strain develops to minimize the Helmholtz free energy.[5–8] The spectrum of phases and domain structures has opened up new applications for thin films. While many of these applications are based on equilibrium properties, new applications will emerge with a better understanding of domain and strain dynamics under nonequilibrium conditions. Because MnAs films grown on Si or GaAs possess periodic structural domains within a large temperature interval,[9–11] we consider them to be an interesting model system to study such dynamics.

Bulk MnAs undergoes a first-order structural-magnetic phase transition at 40 °C, with a thermal hysteresis of 5−10 °C.[12] Below this temperature, in the α phase, MnAs is ferromagnetic with a hexagonal atomic structure (D_{6h} point group). Above 40 °C, in the β phase, MnAs is paramagnetic with an orthorhombic structure (D_{2h} point group).[13] As the temperature increases through the phase transition the $a = b$ lattice constants in the hexagonal plane both abruptly drop nearly equally, by ∼1%, while the c lattice constant along the hexagonal axis varies continuously due to thermal expansion. When MnAs($1\bar{1}00$) is grown epitaxially as a thin film on (001)GaAs at 250 °C, lattice matching can occur with MnAs[0001]||GaAs[$1\bar{1}0$], i.e., with the c axis parallel to the interface.[9,10] Upon cooling below 40 °C the coherently attached film cannot change laterally in size relative to the substrate and elastic stress and strain develop in response to the increase in misfit strain. The phase transition occurs progressively between ∼ 40 and 10 °C. A periodic, or striped, α/β coexistence phase exists as shown schematically in Fig. 1, with the stripes parallel to the c axis. The figure also defines the x, y, z coordinate systems that we use in what follows. Kaganer *et al.*[10] have applied the general analysis of domain formation in thin films by Sridhar *et al.*[5,6] to MnAs films and accounted for many features of the coexistence phase,[11,14] in which the α-phase fraction,[15] ξ, and the saturation magnetization increase monotonically as the temperature drops below 40 °C. The average lateral stress perpendicular to the stripes, σ_{xx}, follows a similar behavior; its temperature dependence[16] is shown in Fig. 2. The stripe period, Λ, which depends on the film thickness, d, as[11,14] $\Lambda \approx 4.8d$, is nearly independent of temperature in the 15–35 °C range. The unusual properties of MnAs thin films have stimulated interest in both fundamental research and applications such as spintronics.[10,11,15,17–19]

Recently we showed how time-resolved optical diffraction from 200 fs to 2 μs following ultrafast optical excitation can be used to reveal the dynamics of the coexistence phase in 150- and 190-nm MnAs thin films.[20] Our goal here is to show how second harmonic generation (SHG) can provide insight into the dynamical strain properties of these thin films following similar excitation conditions. SHG is well known to be sensitive to structural characteristics of crystalline solids and has been used extensively to study bulk and thin film systems.[21,22] Reports of SHG's sensitivity to strain[23–25] suggest that SHG could be a valuable tool for the study of strain dynamics in thin films. Here we demonstrate the sensitivity of SHG to the strain on the MnAs top surface under equilibrium conditions, and with these results as a calibration, we extract the strain dynamics from time-resolved SHG following ultrafast optical pumping. In particular, we demonstrate theoretically and experimentally that SHG is selectively sensitive to only the normal, or yy, component

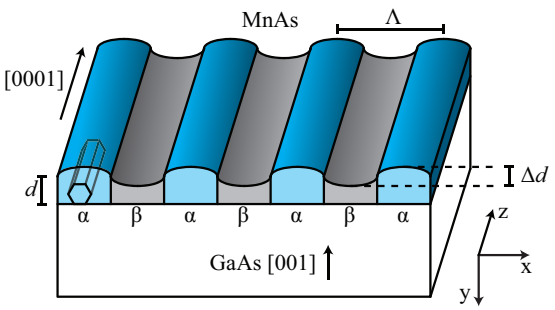

FIG. 1. (Color online) Schematic structure of a MnAs thin film in the coexistence phase.

of surface strain for temperatures from −20 to 70 °C and use this dependence to extract the dynamics of this strain element from time-resolved SHG pump-probe experiments employing 200-fs, 775-nm pulses. We perform time-resolved studies for α-phase films initially at −20 °C as well as for films initially in the coexistence phase at 20 °C. The diffraction and SHG techniques provide complementary information. Whereas SHG provides information on strain at the *top surface*, diffraction is sensitive to the refractive index periodicity and domain height modulation, Δd, where Δd reflects the periodic *vertically integrated* strain field throughout the substrate-film system as governed by the epitaxial constraints. While the two types of experiments provide complementary information about coexistence phase dynamics, only the SHG experiment can provide information about α-phase (strain) dynamics.

The remainder of this paper is organized as follows. In the next section we outline the theoretical considerations supporting the use of SHG to measure surface strain in MnAs films. We also provide a one-dimensional (1D) heat diffusion model to estimate the time-dependent surface temperature following a pump pulse to help interpret the strain dynamics.

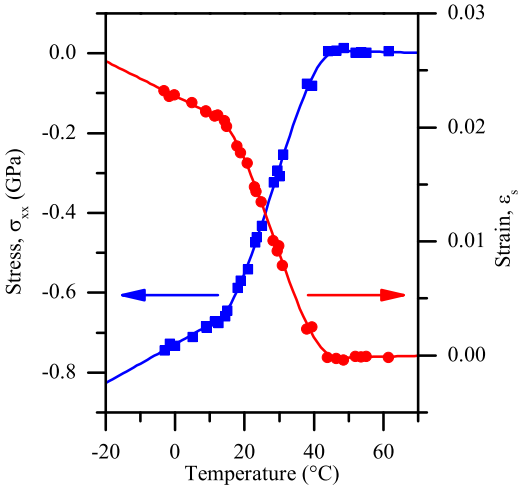

FIG. 2. (Color online) Temperature dependence of the σ_{xx} stress component [(blue) squares] for thin-film MnAs and the derived normal component of the surface strain, ε_s [(red) circles], based on Eq. (6). The curves are guides for the eye. Stress data are reproduced from an earlier work[16] with permission from the American Physical Society and the authors.

Section III provides details on the SHG experimental apparatus and properties of the thin films. Section IV presents the SHG data measured under equilibrium conditions and following optical pumping. The latter results are compared with predictions of the heat diffusion model. Section V offers conclusions about the surface strain studies and, for the coexistence phase, compares the information obtained with that derived from the diffraction experiments.

II. THEORETICAL CONSIDERATIONS

Our objective here is to show how specular SHG from a MnAs thin film is sensitive to the average normal component of the surface strain. We also develop a model for the film's temperature evolution following ultrashort pulse excitation to provide insight into the experimentally obtained time-resolved strain dynamics.

A. Strain-dependent SHG in MnAs films

For a centrosymmetric crystal such as MnAs the dominant sources for SHG are surface electric dipolar and bulk electric quadrupolar in character. While one might also consider magnetization-induced SHG,[26] we neglect it here since we apply no magnetic field and the numerous submicron-size randomly oriented magnetic domains[11,14] yield negligible total/macroscopic magnetization within our much larger optical probing area. On the other hand, an electric quadrupolar source can compete in strength with a surface dipolar contribution if the source volume is large, i.e., for optical absorption depths comparable to or exceeding the optical wavelength. However, the absorption depth for both fundamental and second harmonic light in MnAs is only[17] ∼17 nm. Because of the nonlinear response, the effective e^{-1} escape depth for a bulk SHG signal is ∼6 nm. Hence, we assume bulk and surface quadrupolar SHG sources to be relatively weak and focus on electric dipole effects. Ultimately the experimental results can be used to justify this assumption. However, it is not crucial to our analysis since the influence of strain on both sources is similar. Strain can alter the dipolar source in two possible ways. In the first, an inhomogeneous strain field can remove the inversion symmetry allowing electric dipole SHG to occur. In the second, a homogeneous strain field can modify or induce dipolar surface SHG.[23,24] The strain is expected to be homogeneous along the growth direction because the top of the film cannot expand or contract relative to the bottom of the film. Hence we anticipate that only the surface contribution is operative. In the coexistence phase the periodic component of the strain could, in principle, produce diffracted orders of SHG, but these radiated fields are much weaker than, and certainly do not contribute to, the specular SHG fields considered here.

As shown elsewhere,[23–25] strain-induced electric dipolar SHG is governed by a rank 5 nonlinear photoelastic tensor, $\overline{\mathbf{p}}$, and the total dipolar susceptibility can be written

$$\chi_{ijk} = \chi^0_{ijk} + p_{ijklm}\epsilon_{lm}, \tag{1}$$

where χ^0_{ijk} is the quiescent susceptibility related to an intrinsic source from a strain-free surface. The values of the parameters are *averages* over the optically probed area, which, in our case, is also large compared to Λ. In the absence of external forces,

for a thin film the off-diagonal elements of the total strain tensor are 0.[6] Because of substrate adherence $\epsilon_{xx} = \epsilon_{zz} = 0$; hence, the only nonzero strain tensor element is ϵ_{yy}, which, at the film-air interface, we simply label ε_s. (See Appendix A, which briefly outlines stress/strain properties of MnAs thin films.) The effective surface susceptibility responsible for specular SHG can therefore be written as

$$\chi_{ijk} = \chi^0_{ijk} + p_{ijkyy}\varepsilon_s. \tag{2}$$

We consider only a p-polarized fundamental field E^ω at frequency ω and the p-polarized component of the second harmonic field $E^{2\omega}$, with the plane of incidence making an angle ϕ relative to the film's c axis. Given the twofold rotational symmetry of the MnAs film about the surface normal, the second harmonic field can be written

$$\frac{E^{2\omega}}{(E^\omega)^2} = (a_0 + \varepsilon_s a_s) + (b_0 + \varepsilon_s b_s)\cos(2\phi), \tag{3}$$

where a_0 and b_0 are complex constants related to χ^0_{ijk}, while a_s and b_s are constants related to p_{ijkyy}. The ratio of the second harmonic intensity, $I^{2\omega}$, to the fundamental intensity, I^ω, can therefore be cast in the form

$$\frac{I^{2\omega}}{(I^\omega)^2} = f^{(0)} + f^{(2)}\cos(2\phi) + f^{(4)}\cos(4\phi), \tag{4}$$

where

$$\begin{aligned} f^{(0)} &= |a_0 + \varepsilon_s a_s|^2 + \frac{|b_0 + \varepsilon_s b_s|^2}{2}, \\ f^{(2)} &= 2\Re[(a_0 + \varepsilon_s a_s)(b_0 + \varepsilon_s b_s)^*], \\ f^{(4)} &= \frac{|b_0 + \varepsilon_s b_s|^2}{2}. \end{aligned} \tag{5}$$

Measurements of the temperature-dependent SHG intensity can be used to determine the $a_{0/s}$, $b_{0/s}$ if the temperature-dependent ϵ_s is known. This strain can be obtained either from the temperature dependence of the lattice constants or from the stress in the film (see Appendix A). Because MnAs lattice constant information is available only for the bulk material[11] we use the experimental[16] σ_{xx} thin-film data shown in Fig. 2 to determine the strain. Appendix A shows that ε_s is exactly related to σ_{xx} through

$$\varepsilon_s = -0.031\sigma_{xx}, \tag{6}$$

where stress is measured in gigapascals (GPa); the temperature dependent ε_s is also given in Fig. 2. From the relationship between ε_s and SHG intensity under equilibrium conditions we can interpret time-resolved measurements of SHG following pulsed excitation.

B. Ultrafast heating of MnAs

To determine if the time dependence of ϵ_s following optical pumping is governed by the surface lattice temperature we provide a heat diffusion model to calculate the spatial and temporal dependence of the lattice temperature following pulsed excitation. If MnAs remains entirely in the α or β phase at all times, the temperature can justifiably be determined using suitable optical and thermal parameters in a 1D heat diffusion equation with heat flowing into the MnAs along the y direction. However, when MnAs is initially in the coexistence phase, spatial inhomogeneity of the optical and thermal parameters exists, as well as possible latent heat, enthalpy, and magnetoelastic effects. Furthermore, the theoretical basis for the stripe characteristics has only been formulated under equilibrium conditions,[10] whereas after laser excitation a spatial- and time-dependent temperature occurs. Under these conditions, it is not clear how the stripes and strain field evolve throughout the film and substrate. With insufficient justification to develop a more complex model, we continue to assume a 1D model for heat flow in the coexistence phase using distributed thermal and optical parameters as outlined in Appendix B. Within the approximations listed there, the calculated surface temperature still serves merely as a reference for discussions of ultrafast heating effects in the coexistence phase.

The 1D heat diffusion equation defining a local lattice temperature, T, following optical excitation of a film with specific heat C_P and thermal conductivity K is given by[27]

$$\frac{\partial T}{\partial t} = \frac{1}{C_P}\frac{\partial}{\partial y}\left[K\frac{\partial T}{\partial y}\right] + \Delta T_S \exp(-y/\delta)(1 - e^{-t/\tau_E}), \tag{7}$$

where

$$\Delta T_s = \frac{(1-R)\Phi}{C_P\delta} \tag{8}$$

is the peak increase in surface temperature above the equilibrium temperature, T_0. Here τ_E is the characteristic time for the lattice to establish a temperature following transfer of energy from the optically excited electrons and typically has a value of a few picoseconds,[28] R is the optical reflectivity, δ is the characteristic energy deposition depth in the lattice, and Φ is the pumping pulse fluence. We consider two possible values for δ: a lower limit defined by the optical absorption depth of 17 nm and a value of 40 nm which incorporates an estimated electron ballistic transport distance as discussed in Appendix B. Since the experimental optical pulse width of 200 fs is much less than other characteristic times in Eq. (7) the time dependence of the pulse is not explicitly incorporated. We solve Eq. (7) numerically using the parameters in Appendix B for a 775-nm, s-polarized optical pulse of fluence $\Phi = 1.0$ or 2.0 mJ cm^{-2} incident at 60 $^\circ$ from the normal for which $R = 0.76$. In particular, we obtain the surface temperature, $T(y = 0) = T_s$, which is used to obtain values for ε_s, assuming that the relationship between local temperature and strain is the same as it is under equilibrium conditions.

III. EXPERIMENT

The samples[20] used in the SHG experiments consist of MnAs thin films with $d = 150$ and 190 nm grown on GaAs(001), where MnAs[0001]||GaAs[1$\bar{1}$0]; the thickness was measured using cross-sectional scanning electron microscopy. It was found that the two films gave indistinguishable SHG results to within experimental error; only results from the 150-nm-thick sample are presented here.

Figure 3 shows the experimental arrangement for SHG measurements. The light source is a frequency-doubled Er:fiber oscillator/Ti-sapphire amplifier system that provides 800-μJ, 200-fs, 775-nm pulses at a 1-kHz repetition rate. The

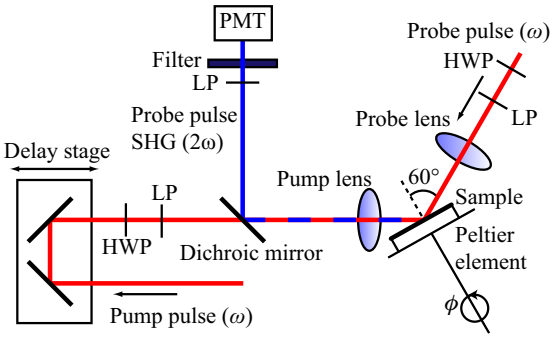

FIG. 3. (Color online) Experimental arrangement used to observe SHG from MnAs thin films. LP, linear polarizer; HWP, half-wave plate; PMT, photomultiplier tube.

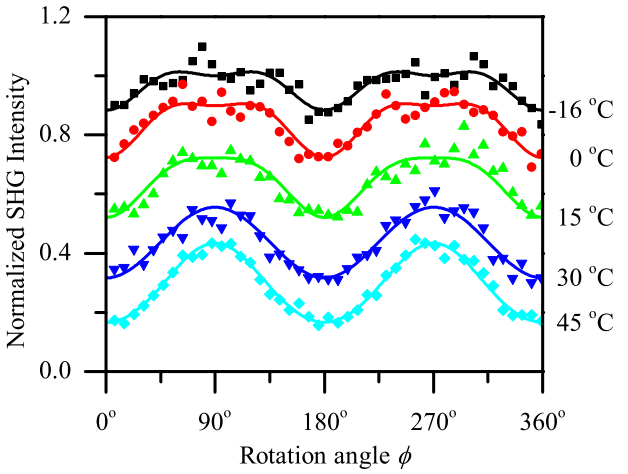

FIG. 4. (Color online) Normalized (see text) SHG intensity from a 150-nm MnAs film on GaAs(001) as a function of azimuthal rotation angle for several values of the equilibrium temperature, T_0. The solids curves are fits based on Eq. 4.

p-polarized probe pulses are focused onto the sample at 60° with a 20-cm-focal-length lens, and p-polarized SHG light is collected with a 5-cm-focal-length lens. The s-polarized pump pulses follow the same beam path in the opposite direction and are focused with a 5-cm lens. Both lenses are defocused by 2 mm to generate a probe spot size of 220 × 40 μm (FWHM) and pump spot size of 300 × 180 μm. The peak pump fluence at the center of the pump spot is either $\Phi = 1.0$ or 2.0 mJ cm^{-2}, hereafter referred to as low and high fluence. The probe fluence is $\leqslant$1 mJ cm^{-2}. During its 200-fs duration lattice heating is insignificant since probe energy has yet to be transferred to the lattice. Hence the probe can be considered nonperturbative. The 388-nm SHG light is separated from the fundamental pump and probe light with a dichroic mirror, optically filtered, and measured using a cooled photomultiplier with photon counting electronics. The pump beam contains a delay arm to introduce pump-probe delays, τ, up to 675 ps. A linear polarizer and half-wave plate are used to control the polarization of the fundamental probe beam, and another polarizer is used as an analyzer.

Samples are mounted on a rotational stage and the SHG intensity is measured as a function of the azimuthal angle, ϕ. The equilibrium temperature, T_0, is monitored using a thermocouple mounted on the sample side and a thermoelectric cooler is used to maintain a temperature between −20 and 70 °C. Samples are enclosed in a dehumidified chamber to prevent condensation and minimize surface contamination.

IV. RESULTS AND DISCUSSION

A. Determination of surface strain from temperature-dependent SHG

The ϕ dependence of the SHG intensity was measured in the absence of a pump beam for 20 values of T_0, beginning at −20 °C and stopping at 70 °C. Results obtained during sample cooling displayed the expected thermal hysteresis effects. At each temperature the SHG intensity is fitted using Eq. (4) to obtain values for $f^{(0)}$, $f^{(2)}$, and $f^{(4)}$; the SHG intensity is normalized such that the highest value for the isotropic term, $f^{(0)}$ (obtained at −20 °C), is unity. Representative SHG data and corresponding fits are shown in Fig. 4 for six values of T_0. The values of $f^{(0)}$, $f^{(2)}$, and $f^{(4)}$ for all temperatures are shown in Fig. 5. From fits to these coefficients using the strain data in Fig. 2 we obtain the $a_{0/s}$ and $b_{0/s}$ constants. However, their values are not given here since they lack physical significance. To within experimental error a good fit is obtained for each of the three coefficients.

The data in Fig. 5, especially for $f^{(0)}$, show the trends expected from the theoretical basis for strain-induced SHG. The $f^{(0)}$ component (azimuthal average) of the SHG signal is lowest at 40 °C, where the strain is lowest, increases with decreasing temperature through the coexistence phase, and increases more slowly below 10 °C. Above 40 °C, the SHG intensity increases only slightly, if at all. The nearly strain-free SHG signal in this regime is a measure of the quiescent susceptibility term in Eq. (1). Overall, the temperature-dependent behavior of the SHG signal correlates well with that of ε_s shown in Fig. 2. The $f^{(0)}$, $f^{(2)}$, and $f^{(4)}$ coefficients all give remarkably close agreement, validating the assumption that the SHG signal is being modified by surface strain. Using these results as a calibration of the ε_s dependence of SHG we now consider surface strain dynamics following ultrafast optical pumping.

B. Determination of surface strain from time-dependent SHG following optical pumping

For the pump-probe experiments three cases are investigated:

(i) high Φ, with the sample initially at $T_0 = -20$ °C, where the film is initially in the α phase and the calculated surface temperature peaks near 10 °C, the onset of the coexistence phase;

(ii) low Φ, with $T_0 = -20$ °C, whereby the MnAs should remain in the α phase; and

(iii) high Φ, with $T_0 = 20$ °C, for which the film is initially in the coexistence phase.

In each case the ϕ-dependent SHG intensity was measured for discrete values of τ up to 675 ps. For case 1, which gives the largest pump-induced change in SHG intensity, the data for each τ were fit using Eq. (4) to obtain values of $f^{(0)}$,

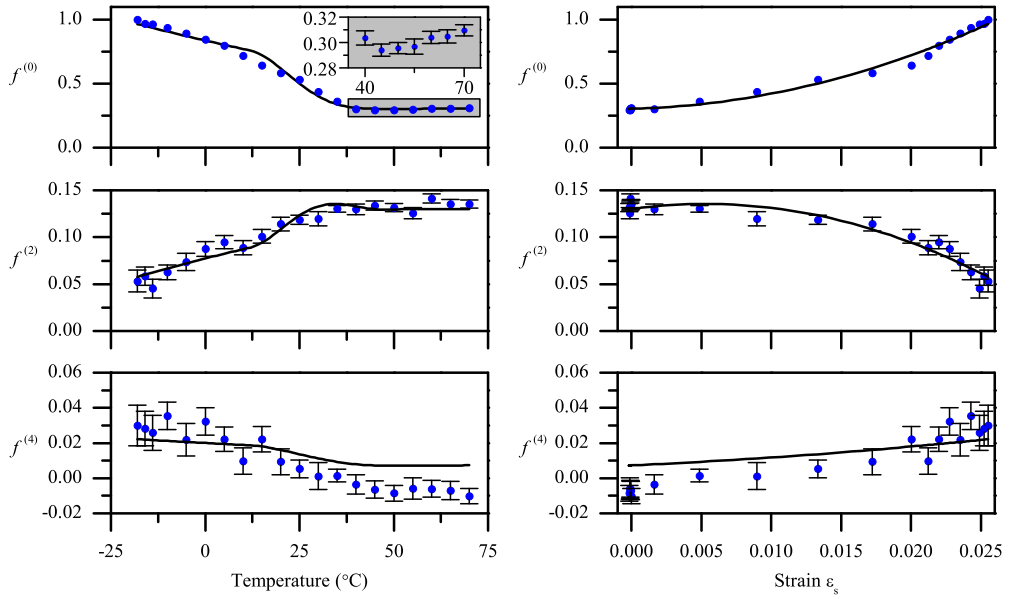

FIG. 5. (Color online) The $f^{(0)}$, $f^{(2)}$, and $f^{(4)}$ coefficients of SHG intensity as a function of temperature (left) and surface strain (right) for the 150-nm MnAs film. Inset for $f^{(0)}$: details beyond 40 °C. Curves are fits based on fits to Eq. (4). Error bars have the same magnitude for all coefficients but are discernible only for $f^{(2)}$ and $f^{(4)}$.

$f^{(2)}$, and $f^{(4)}$. These are shown in Fig. 6. The $f^{(0)}$ element decreases to a minimum value within several picoseconds, consistent with a decrease in ε_s and the expected increase in T_s. Both temperature and strain partially recover towards their equilibrium values over hundreds of picoseconds. The $f^{(2)}$ and $f^{(4)}$ elements have a much lower signal/noise ratio but suggest the same trend. The curves shown in the graphs indicate that the three coefficients give a consistent time-dependent ε_s as they did under equilibrium conditions. Since $f^{(0)}$ shows the clearest trends, it is the only one considered further.

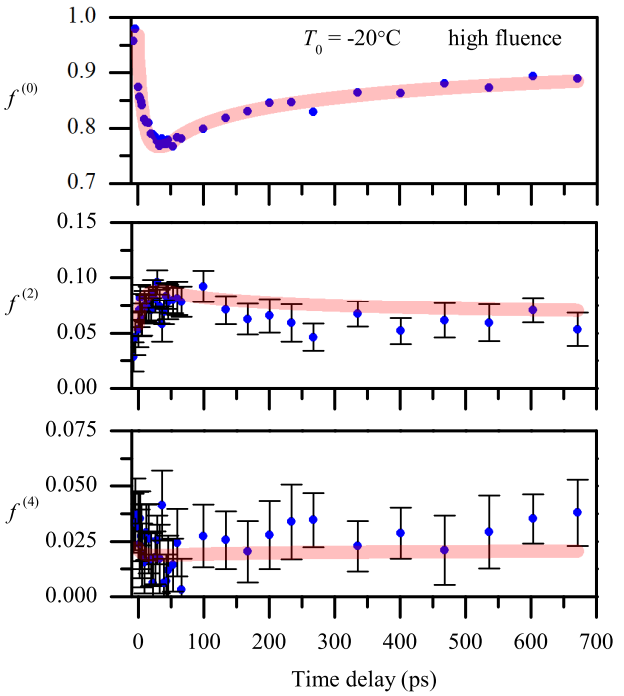

FIG. 6. (Color online) Time-delay-dependent $f^{(0)}$, $f^{(2)}$, and $f^{(4)}$ coefficients obtained from the SHG intensity for a 150-nm MnAs film initially at $T_0 = -20\,^{\circ}$C and optically excited at high fluence. Error bars have the same magnitude for all three components and are only apparent for the $f^{(2)}$ and $f^{(4)}$ elements. Shaded (red) curves show that the three coefficients give a consistent value for surface strain or temperature, based on the data in Fig. 5.

It is shown in Fig. 5 that there is a one-to-one correspondence (neglecting data for $T_0 > 40\,^{\circ}$C) between $f^{(0)}$ and T_0 or between $f^{(0)}$ and ε_s. Figure 7 shows the extracted time-dependent ε_s for case 1. The ε_s clearly drops after excitation but stays above 0.02, indicating that the top surface of the film just reaches a temperature corresponding to the lower boundary of the coexistence phase. From the relation between ε_s and temperature implied by Fig. 2 the T_s can be determined and this is shown in the lower panel in Fig. 7. The figure also shows the time dependence of T_s and associated ε_s calculated using Eq. (7) for $\delta = 17$ and 40 nm. The initial behavior of the time-dependent ε_s is best fit using a τ_E of approximately 5 ps, which is consistent with typical electron-lattice thermalization times in metals as discussed in Appendix B. With these parameters, there is reasonable agreement between the value of ε_s extracted from the experiments and that determined from the 1D heat diffusion model. In particular, the dependence of ε_s for long times is consistent with the time dependence of the surface temperature up to 675 ps, by which time the thermal diffusion length attains a value of ~45 nm (see Appendix B), still much smaller than the film thickness. Certainly small adjustments to the model parameters such as δ could be used to improve the fit, but this may not be meaningful in view of the uncertainty in the precise value of all experimental parameters.

The extracted ε_s and T_s for case 2 are shown in Fig. 8, with the values presented in the same manner as for case 1. The upper graph shows the extracted ε_s, and the lower graph

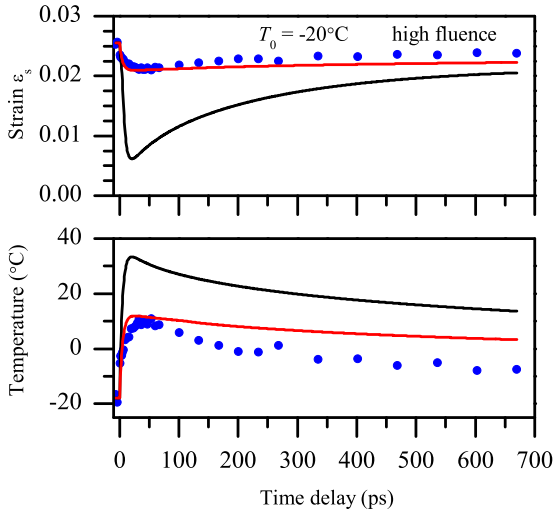

FIG. 7. (Color online) Extracted ε_s and corresponding surface temperature [(blue) circles] as a function of the time delay after optical excitation at high fluence of a sample initially at $-20\,^{\circ}$C. Also shown are the calculated corresponding surface temperature and temperature-dependent surface strain obtained from the heat diffusion model for $\delta = 17$ nm (black curves) and $\delta = 40$ nm [lighter (red) curves].

shows the extracted T_s, assuming that the relationship between the two quantities is the same as in the equilibrium case; the T_s values calculated from Eq. (7) and associated ε_s are shown for the two possible values of δ with $\tau_E = 5$ ps. Again, the calculations of T_s and ε_s based on $\delta = 40$ nm fit the data reasonably well.

From cases 1 and 2 we find that time-resolved SHG experiments enable extraction of the surface strain dynamics

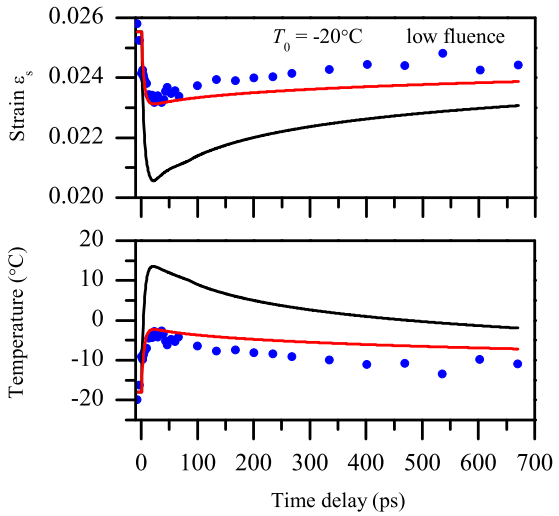

FIG. 8. (Color online) Extracted ε_s and corresponding surface temperature [(blue) circles] as a function of the time delay after optical excitation at low fluence of a sample held at $T_0 = -20\,^{\circ}$C. Also shown are the corresponding surface temperature and temperature-dependent surface strain values obtained from the heat diffusion model assuming $\delta = 17$ nm (black curves) and $\delta = 40$ nm [lighter (red curves)].

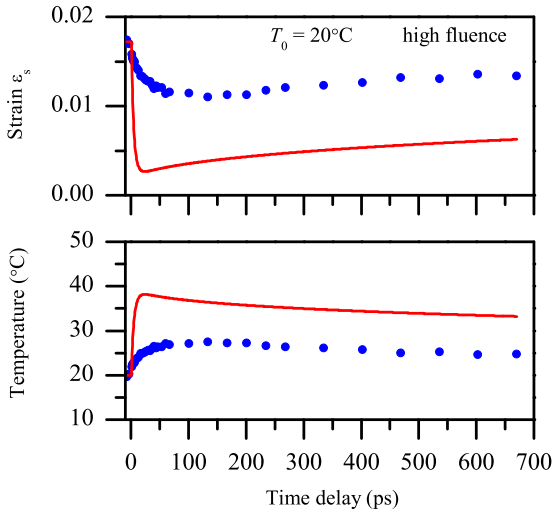

FIG. 9. (Color online) Extracted surface strain, ε_s, and corresponding surface temperature [(blue) circles] as a function of the time delay after optical excitation of a film at $T_0 = 20\,^{\circ}$C and pumped with a high fluence. Curves show the surface strain and temperature derived from the heat diffusion model using $\delta = 40$ nm.

and the extracted ε_s values are in reasonable agreement with a model which relates this strain to the surface temperature obtained from a 1D heat diffusion model. The extracted ε_s and T_s for a high pump fluence with the sample initially at $T_0 = 20\,^{\circ}$C (case 3) are shown in Fig. 9. As in the previous cases ε_s and T_s initially decrease and increase, respectively, towards an extremum and subsequently return towards their equilibrium values over hundreds of picoseconds. However, ε_s initially falls on a 100-ps time scale, much longer than that observed when the film is initially at $T_0 = -20\,^{\circ}$C. This is probably too long to be attributed to electron-lattice thermalization, which should not depend significantly on which phase or combination of phases is involved. The fall time is likely related to the time for latent heat acquisition of the α-phase components or to stripe dynamics.[20] Such a long time is not unexpected since a characteristic time of $\sim$100 ps for structural transformation associated with first-order phase transitions has also been reported elsewhere.[29] Also, as found in earlier diffraction experiments,[20] the stripe dynamics are very complex on a time scale of several hundred picoseconds, reflecting misfit and elastic strain temporal-spatial behavior throughout the film under these highly nonequilibrium conditions.

The curves in Fig. 9 show the calculated T_s and ε_s using $\delta = 40$ nm. For $\tau > 100$ ps, although the thermal model employing the distributed thermal parameters for the coexistence phase (see Appendix B) gives a recovery time which represents the data reasonably well, clearly the values of the calculated and measured ε_s or T_s do not agree. When the sample initially at $T_0 = 20\,^{\circ}$C is excited by the low-fluence pump pulse, the decrease (increase) in surface strain (temperature) is approximately half that produced by the high-fluence pump but otherwise shows characteristics similar to those of the high-fluence case, including significant discrepancies from calculated values. For both low and high fluence the discrepancy between the data and the model calculations may

be due to the assumed parameters in the model or its 1D character, especially in view of the existence of stripes and their dynamics.[20] Given the long time taken for ε_s to change in the coexistence phase and the fact that ε_s never reaches values consistent with the calculated surface temperature, it is likely that ε_s under these nonequilbirium conditions is not governed by the surface temperature alone. The *entire* strain field under such conditions likely also depends on constraints *throughout* the film/substrate system including the MnAs/GaAs interface, as it does under equilibrium conditions.[10]

V. CONCLUSIONS

In summary, we have measured optical SHG from 150- and 190-nm $(1\bar{1}00)$MnAs thin films on GaAs(001) under equilibrium conditions and following ultrafast optical pulse excitation with the film initially either in the α phase or in the coexistence phase. For equilibrium conditions the SHG azimuthal angle and temperature dependence are shown experimentally and theoretically to be sensitive to the spatially averaged normal component of the surface strain. When a film is excited with an ultrashort laser pulse, the angle-independent component of the SHG intensity decreases on a few-picosecond time scale as the surface temperature increases and the surface strain decreases. For films initially in the α phase at $-20\,^{\circ}$C the characteristic time for the minimum strain to be reached, $\sim$5 ps, is consistent with electron-lattice thermalization. The strain then recovers towards its equilibrium value over several hundred picoseconds. The extracted strain time dependence is consistent with calculations based on a 1D heat diffusion model with an initial energy deposition depth of $\sim$40 nm which incorporates ballistic electron transport. For a film initially in the coexistence phase at 20 °C, the strain requires $\sim$100 ps to reach its minimum value, possibly due to first-order phase transition dynamics, including latent heat accumulation. The drop in strain, however, is much less than that predicted by the heat diffusion model, evidence either of shortcomings of the 1D model or that the average surface strain is not governed by the (local) surface temperature alone under nonequilibrium conditions.

Finally, we comment on the differences between the time-resolved SHG and diffraction experiments[20] for the coexistence phase. Differences are not unexpected since the two experiments measure different properties of the strain field, as stated towards the end of Sec. I. The diffraction experiments show how optical pumping of the coexistence phase perturbs the periodic strain field *throughout* the film/substrate system, producing oscillations in the α/β-phase fraction via a standing acoustic wave with a period of hundreds of picoseconds, dependent on the film thickness. The specular SHG experiments give results independent of the film thicknesses we used and show how the spatially averaged normal component of the surface strain, not directly sensitive to phase periodicity, falls on a 100-ps time scale and then begins to recover monotonically on a 500-ps time scale. These results indicate how the two techniques, one (specular SHG) sensitive to the zeroth-order Fourier component (spatial average) of the surface strain and the other (diffraction) sensitive to the first-order Fourier component of the integrated strain-field modulation amplitude, reveal different sides of the dynamics of the coexistence phase.

ACKNOWLEDGMENTS

We thank Dave Rench and Nitin Samarth of the University of Pennsylvania for providing the MnAs thin films used in these studies, as well as Kenneth Burch for helpful discussions. We acknowledge financial support from the NSERC (Canada) and C.L. acknowledges partial financial support from the Alexander von Humboldt Foundation.

APPENDIX A: STRESS AND STRAIN IN MnAs

In general, a MnAs film is composed of α and β phases with fractions ξ and $1-\xi$, respectively. The total (tensor) strain in the film, $\overline{\epsilon}$, is the sum of the elastic, $\overline{\mathbf{e}}$, and misfit, $\overline{\eta}$, strain for the appropriate phases. Because of the hexagonal symmetry of the MnAs for which there is no shear stress, all off-diagonal elements of $\overline{\epsilon}$, $\overline{\mathbf{e}}$, and $\overline{\eta}$ are 0. Since the MnAs film is fixed in the x-z plane by the substrate, the xx and zz components of the total strain averaged over this plane are 0. Therefore, the only nonzero component of the spatially averaged total strain is ϵ_{yy}, and the film can only expand along the normal direction. If $\overline{\sigma}$ is the stress tensor, since the sample is free to expand in the y direction, the yy component of the spatially averaged stress, σ_{yy}, vanishes. Finally, since the orthorhombic distortion is minimal, the misfit strains in the x and y directions are equal. To summarize,[10]

$$\begin{aligned}
\epsilon_{ii}^{\alpha,\beta} &= e_{ii}^{\alpha,\beta} + \eta_{ii}^{\alpha,\beta},\\
\epsilon_{xx} &= \xi\epsilon_{xx}^{\alpha} + (1-\xi)\epsilon_{xx}^{\beta} = 0,\\
\epsilon_{zz} &= \xi\epsilon_{zz}^{\alpha} + (1-\xi)\epsilon_{zz}^{\beta} = 0,\\
\eta_{xx}^{\alpha,\beta} &= \eta_{yy}^{\alpha,\beta} \neq \eta_{zz}^{\alpha,\beta},\\
\sigma_{yy} &= 0.
\end{aligned} \tag{A1}$$

Hooke's law can be written as $\sigma_{ij} = c_{ijkl}e_{kl}$, where c_{ijkl} are the components of the elastic modulus tensor. Because of the hexagonal symmetry, the x and y directions are equivalent so that $c_{xxzz} = c_{yyzz}$, etc. The four independent elastic constants are[30] $c_{xxxx} = 40$ GPa, $c_{zzzz} = 110$ GPa, $c_{xxyy} = 8$ GPa, and $c_{xxzz} = 10$ GPa. The ϵ_{yy} can be obtained from Hooke's law and Eq. (A1) using the values of σ_{xx} from the literature.[16] One finds

$$\epsilon_{yy} = \frac{1}{c_{xxyy} - c_{xxxx}}\sigma_{xx} = -0.031\sigma_{xx}, \tag{A2}$$

where stress has units of gigapascals.

APPENDIX B: PARAMETERS FOR THE HEAT DIFFFUSION MODEL

The 1D heat diffusion equation, Eq. (7), is solved using parameters obtained from the literature and the usual boundary conditions. We discuss the parameters here.

(i) *Optical parameters*. The optical penetration depth of MnAs at 775 nm is obtained from the ordinary dielectric constant, which, for the α and β phases, is given by[17] $\epsilon_o^{\alpha} = -6 + 19i$ and $\epsilon_o^{\beta} = -1 + 23i$. This gives ordinary

refractive indices of $n_o^\alpha = 2.6 + 3.6i$ and $n_o^\beta = 3.3 + 3.5i$, respectively. The extraordinary indices are similar in value. From the optical constants the reflectivity of an s-polarized beam incident at 60 ° is $R = 0.76$. The optical penetration depth is $\frac{\lambda}{4\pi\Im(n_o^{\alpha,\beta})} \sim 17$ nm. Alternatively, from Stoffel *et al.*[31] one finds $n = 2 + 2.8i$, which yields an optical penetration depth of 22 nm. However, the optical penetration depth is the lower limit of the energy deposition depth in the lattice, δ. When electrons are optically excited they can move ballistically before interacting with the lattice. In good metallic films such as gold, the ballistic length is ∼100 nm.[32] In poor metals the ballistic length is ∼30 nm.[33] In solving Eq. (7) we have considered δ with values of 17 and 40 nm, reflecting a reasonable range for the energy deposition depth.

(ii) τ_E. In the homogeneous α phase the time taken for the lattice temperature (and lattice constants) to change in response to optical excitation is taken to be ∼5 ps, consistent with values given in the literature.[28] Note, however, that this time may be much longer if there is a phase change which accompanies energy deposition. Indeed, it is well known[29] that it may take hundreds of picoseconds for the latent heat to be released during a first-order phase transition. Hence this longer time might be more appropriate when the coexistence phase is excited.

(iii) *Thermal parameters*. Detailed thermal properties of thin-film MnAs are not available and so we are guided by the bulk properties. Near room temperature but away from the 40 °C phase transition, MnAs has a heat capacity of[34] 5.6×10^7 J mol^{-1} K^{-1}, which, for a MnAs mass density of 6.4×10^3 kg m^{-3}, is equivalent to a heat capacity at constant pressure of 2.8×10^6 J m^{-3} K^{-1}; the heat capacity increases as the transition is approached. The latent heat is[35] $L = 4.7 \times 10^7$ J m^{-3}. In the thin-film coexistence phase we consider that the latent heat is distributed between 10 and 40 °C. We therefore add $L\frac{d\xi}{dT}$ to the bulk specific heat in the α phase. In the temperature range 15 to 35 °C, where ξ drops linearly with temperature, this gives a constant effective heat capacity of 5.2×10^6 J m^{-3} K^{-1}. The thermal conductivity, K, of bulk MnAs[35] is nearly independent of temperature in the range of interest, with a value of 2.0 W m^{-1} K^{-1}. The thermal diffusivity, $\kappa = K/C_P$, away from the phase transition therefore has a value of $\sim 6.7 \times 10^{-7}$ m^2 s^{-1}, which agrees well with the value obtained elsewhere.[35] For this κ the thermal diffusion length $2\sqrt{\kappa\tau} = 45$ nm for $\tau = 675$ ps and heat diffusion across the MnAs/GaAs interface is negligible on the time scale of interest here. In particular, the surface temperature is insensitive to the presence of that interface, which is ignored in our calculations. Equation (7) is subject to the boundary conditions that initially the entire film is at temperature T_0 and heat flow across the MnAs top surface is always absent, or

$$\frac{\partial T(y,t)}{\partial y} = 0 \quad \text{at} \quad y = 0. \tag{B1}$$

Equation (7) can be solved numerically using a finite-difference method with the temperature-dependent values of C_P and K.

*vandriel@physics.utoronto.ca

[1] R. Ramesh and N. A. Spaldin, Nature Mater. **6**, 21 (2007).
[2] R. von Helmolt, J. Wecker, B. Holzapfel, L. Schultz, and K. Samwer, Phys. Rev. Lett. **71**, 2331 (1993).
[3] D. Schlom, L.-Q. Chen, C.-B. Eom, K. Rabe, S. Streiffer, and J.-M. Triscone, Annu. Rev. Mater. Res. **37**, 589 (2007).
[4] C. Eom *et al.*, Nature **411**, 558 (2001).
[5] N. Sridhar, J. M. Rickman, and D. J. Srolovitz, Acta Mater. **44**, 4085 (1996).
[6] N. Sridhar, J. M. Rickman, and D. J. Srolovitz, Acta Mater. **44**, 4097 (1996).
[7] A. L. Roytburd, J. Appl. Phys. **83**, 228 (1998).
[8] A. L. Roytburd, J. Appl. Phys. **83**, 239 (1998).
[9] V. M. Kaganer, B. Jenichen, F. Schippan, W. Braun, L. Daweritz, and K. H. Ploog, Phys. Rev. Lett. **85**, 341 (2000).
[10] V. M. Kaganer, B. Jenichen, F. Schippan, W. Braun, L. Daweritz, and K. H. Ploog, Phys. Rev. B **66**, 045305 (2002).
[11] L. Däweritz, Rep. Prog. Phys. **69**, 2581 (2006).
[12] B. T. M. Willis and H. P. Rooksby, Proc. Phys. Soc. B **67**, 290 (1954).
[13] R. H. Wilson and J. S. Kasper, Acta Cryst. **17**, 95 (1964).
[14] L. Däweritz, L. Wan, B. Jenichen, C. Herrmann, J. Mohanty, J. Trampert, and K. H. Ploog, J. Appl. Phys. **96**, 5056 (2004).
[15] T. Plake, T. Hesjedal, J. Mohanty, M. Kästerner, L. Däweritz, and K. H. Ploog, Appl. Phys. Lett. **82**, 2308 (2003).
[16] A. K. Das, C. Pampuch, A. Ney, T. Hesjedal, L. Däweritz, R. Koch, and K. H. Ploog, Phys. Rev. Lett. **91**, 087203 (2003).
[17] B. Gallas, J. Rivory, H. Arwin, F. Vidal, and V. H. Etgens, Phys. Stat. Solidi A **205**, 859 (2008).
[18] B. R. Salles, F. Vidal, V. Etgens, R. Breitwieser, M. Marangolo, and M. Eddrief, Physics B **404**, 2684 (2009).
[19] R. Breitweiser, F. Vidal, I. L. Graff, M. Marangolo, M. Eddrief, J.-C. Boulliard, and V. H. Etgens, Phys. Rev. B **80**, 045403 (2009).
[20] J. J. Dean, D. W. Rench, N. Samarth, and H. M. van Driel, Phys. Rev. Lett **111**, 035701 (2013).
[21] Y. R. Shen, Nature **337**, 519 (1989).
[22] J. J. Dean and H. M. van Driel, Phys. Rev. B **82**, 125411 (2010).
[23] L. Kulyuk, D. A. Shutov, E. E. Strumban, and O. A. Atktsipetrov, J. Opt. Soc. Am. B **8**, 1766 (1991).
[24] D. J. Bottomley, A. Mito, P. Fons, S. Niki, and A. Yamada, IEEE J. Quant. Elec. **33**, 1294 (1997).
[25] I. L. Lyubchanskii, N. N. Dadoenkova, M. I. Lyubchanskii, Th. Rasing, J.-W. Jeong, and S.-C. Shin, Appl. Phys. Lett. **76**, 1848 (2000).
[26] R.-P. Pan, H. D. Wei, and Y. R. Shen, Phys. Rev.B **39**, 1229 (1989).
[27] H. S. Carslaw and J. C. Jaeger, *Conduction of Heat in Solids* (Oxford University Press, New York, 1986).
[28] N. Rotenberg, A. D. Bristow, M. Pfeiffer, M. Betz, and H. M. van Driel, Phys. Rev.B **75**, 155426 (2007).

[29]M. K. Liu, B. Pardo, J. Zhang, M. M. Qazilbash, S. J. Yun, Z. Fei, J.-H. Shin, H.-T. Kim, D. N. Basov, and R. D. Averitt, Phys. Rev. Lett. **107**, 066403 (2011).
[30]M. Dörfler and Bärner, Phys. Status Solidi A **17**, 141 (1973).
[31]A. M. Stoffel and J. Schnedier, J. Appl. Phys. **41**, 1405 (1970).
[32]S. D. Brorson, J. G. Fujimoto, and E. P. Ippen, Phys. Rev. Lett. **59**, 1962 (1987).
[33]J. Hohlfield, S.-S. Wellershoff, J. Güdde, U. Conrad, V. Jähnke, and E. Matthias, Chem. Phys. **251**, 237 (2000).
[34]J.-W. Schünemann, A. Lange, G. A. Govor, K. Bärner, and E. Gmelin, J. Alloys Compd. **178**, 237 (1992).
[35]S. Fujeida, Y. Hasegawa, A. Fujita, and K. Fukamichi, J. Appl. Phys. **95**, 2429 (2004).